IEEE Access
Multidisciplinary | Rapid Review | Open Access Journal

Received February 19, 2020, accepted March 14, 2020, date of publication March 23, 2020, date of current version April 7, 2020.

Digital Object Identifier 10.1109/ACCESS.2020.2982802

Extended Hermite Radial Basis Functions for Sparse Contours Interpolation

DEYUN ZHONG[1,2], LIGUAN WANG[1,2], AND LIN BI[1,2]
[1]School of Resources and Safety Engineering, Central South University, Changsha 410083, China
[2]Research Center of Digital Mine, Central South University, Changsha 410083, China

Corresponding author: Lin Bi (mr.bilin@csu.edu.cn)

This work was supported in part by the National Key Research and Development Program of China under Grant 2017YFC0602905, and in part by the National Natural Science Foundation of China under Grant 41572317.

ABSTRACT In this paper, we present an extended Hermite radial basis functions interpolant for surface reconstruction of sparse contours that allows for shape control with interactive constraints. Similar to the differential operator, the difference operator is used to construct gradient constraint and tangent constraint. Based on the theory of Hermite-Birkhoff interpolation, to construct more flexible geometry constraints, we incorporate the differential operator and difference operator to construct interpolation conditions in the interpolant. We construct some constraint rules to control the local trend of shape interactively. It is useful when the method interpolates sparse data that satisfies all the constraints but exhibits an undesirable trend of shape. For example, the interactive constraints can be used to fix holes or intersections for geometrically valid meshes. Regarding the geometry domain as a signed distance field of implicit function, we implement a constraint-based approach to interpolate the contours using the interpolant. The improved method can flexibly handle both parallel and non-parallel sparse contours. The numerical results of real geological and medical data show the robustness and performance of the extended Hermite radial basis functions interpolant.

INDEX TERMS Hermite radial basis functions, radial basis functions, contours interpolation, signed distance field, geometry constraints.

I. INTRODUCTION

Surface reconstruction of parallel or non-parallel cross sections using radial basis functions (RBFs) is widely used in the fields of geological interpretation (e.g., orebody contours within parallel sections), medical engineering, and geometric processing. This involves the problem of multivariate scattered data approximation, especially recovering an unknown implicit function from sparse contours to reconstruct a desired surface.

However, the problem of inferring an implicit surface from sparse contours is a non-trivial task. It requires not only a minimal error in approximation but also a desired shape in geometry. A set of sparse sections provides little information about the local topology of the multiple contours to explore the shape trend. It is a notoriously ill-posed problem, since the type of contours data is often sparse, and hence requires much extrapolation. For sparse data (e.g., sparse contours), it is necessary to develop an implicit surface reconstruction method with flexible interactive constraints. To be useful for applications, more importantly, the same data has to meet different correctness criteria in different circumstances. For example, the stitching of multiple contours in adjacent sections has different extrapolation rules and topological connections. Therefore, the contours need to have different constraint rules, and the modeling method may need to dynamically adjust the local constraint rules to adapt to the different application requirements.

We try to interpolate the sparse contours by improving the Hermite-Birkhoff interpolation using radial basis functions. The RBF-based interpolants can easily generate the isosurface from dense point clouds, with a lack of interactive tools, so it is more suitable for modeling dense data. To avoid approximating the normals by offsetting points, the Hermite radial basis functions (HRBF) interpolant [1], [2] is developed to exactly interpolate the first-order Hermite data (known as gradient constraints). The problem of Hermite-Birkhoff interpolation of scattered data using radial basis functions is further investigated to satisfy more interpolation constraints. This extended problem is also

The associate editor coordinating the review of this manuscript and approving it for publication was Yue Zhang.

called as generalized interpolation by Wendland [3], and Hermite Radial Basis Functions Implicits are indeed a special case of the generalized interpolation theory [1].

In this paper, we present an extended Hermite radial basis functions (EHRBF) interpolant for enforcing shape trends and topological constraints when reconstructing surfaces from sparse contours. Similar to the differential operator (vector type, with three components), the difference operator (scalar type) [4] is used to construct gradient constraint and tangent constraint. For example, the tangent constraint constructed by difference operator can be also used to change the local trend of shape. It is useful to fix holes or intersections for geometrically valid meshes. To construct more flexible geometry constraints, we incorporate the differential operator and difference operator to construct interpolation conditions in the interpolant.

There are many applications for the RBF-based methods with extended constraints in surface reconstruction. Similar to the generalized radial basis functions interpolant (GRBF), based on the interpolation constraints, some interactive constraints [5], including the trend line and the constraint line, can be constructed to control the local trend of shape interactively. It is useful when the method interpolates sparse data that satisfies all the constraints but exhibits an undesirable trend of shape. In orebody modeling, the interactive constraints are used to interpolate sparse drillholes and to construct geology rules [5]. In this paper, the EHRBF interpolant is used to interpolate sparse contours. To interpolate the contours, the geometry domain is viewed as a signed distance field [6] of implicit function and the implicit surface can be extracted using the Marching Cubes method [7]. This approach of surface reconstruction is known as implicit modeling [8] in geometry processing. The numerical results of real geological and medical data show the robustness and performance of the EHRBF interpolant.

The outline of this paper is as follows. We first review some preliminary knowledge about generalized interpolation theory, and then present the extended Hermite Radial Basis Functions interpolant in Section II. Section III presents the improved method of implicit modeling from sparse cross sections, including some constraint rules. The experimental results and comparisons are demonstrated in Section IV. We conclude the paper in the last section with some future research problems.

A. RELATED WORKS

The problem of radial basis functions interpolation has been widely studied in the past two decades. Two bodies of work are briefly reviewed, namely Hermite-Birkhoff interpolation and contours interpolation.

The possibility of Hermite interpolation using radial basis function was first introduced by Wu [9] in 1992. Since then, this topic has been further investigated significantly. The data types are extended to interpolate some linear functional data and the corresponding interpolant is called a generalized interpolant. The HRBF interpolant can be viewed as a special case of the generalized interpolant. In more general situation, the domain constraints and the gradient constraints of the HRBF interpolant can be interpolated in the same points. Based on the Hermite-Birkhoff interpolation theory with RBFs, Macedo *et al.* [1] derived HRBF Implicits to interpolate implicit surface. To accelerate the speed of solution, they replaced the globally-supported RBFs with compactly-supported RBFs. Instead of interpolating all pairs of point-normals, Harlen *et al.* [10] selected a small subset of point-normals as interpolation centers using adaptive greedy method. Further, Liu *et al.* [11] proposed a closed-form HRBF method to solve the efficiency problem of surface reconstruction using quasi-interpolation techniques.

The approach is the closest to the class of methods that extend the constraints of the RBF-based interpolant [12], [13] to interpolate the geometry domain as an implicit function. Based on the theory of Hermite-Birkhoff interpolation with radial basis functions, some generalized interpolants with different interpolation constraints are developed, including the anisotropic radial basis functions (ARBF) interpolant [14], the generalized radial basis functions (GRBF) interpolant [15] and the generalized Hermite radial basis functions (GHRBF) interpolant [16]. Gois *et al.* [17] applied the GHRBF to reconstruct implicit surface from polygonal meshes. Liu *et al.* [18] utilized the ARBF to interpolate images with local feature orientations (anisotropic intensities). In this work, we extend the general constraints based on the theory of generalized interpolation to interpolate the implicit surface for additional flexibility.

The methods of surface reconstruction from contours can be divided as explicit modeling and implicit modeling. In contrast to the explicit modeling, such as the Delaunay triangulation from cross-section curves [19], the implicit modeling defines the wireframe-free surface with constraints by an implicit function, which is easy to dynamically update the meshes. Note that the method using projection strategy proposed by Liu *et al.* [20] may also be considered as an explicit modeling method in fact. Several implicit functions such as Moving Least Squares [21], harmonic functions [22], mean-value interpolation [23] and radial basis functions can be used to interpolate an implicit surface. However, the current implicit functions are often used for surface reconstruction from dense data, particular dense point clouds, lacking the necessary interactive constraint tools.

We mainly focus on three aspects of the reconstruction methods. For normal estimation, Ijiri *et al.* [24] improved the previous estimation method, and proposed a novel contour-based volume image segmentation technique using Bilateral Hermite Radial Basis Functions (B-HRBF). For contours interpolation, several signed scalar field methods such as RBF, HRBF and harmonic functions are used in the implicit modeling of contours. By defining multi-labeled implicit function, Huang *et al.* [25] extended the topology-controlled reconstruction algorithm of Zou *et al.* [22] to reconstruct multi-labeled material interfaces from cross-sections. Kim *et al.* [26] developed an energy minimization

model with constraints for the accurate surface reconstruction from parallel cross sections. However, these methods lack effective constraint rules to control the shape trend and topology relationships. For interpolation constraints, apart from incremental sampling (e.g. Zou *et al.* [22]), template-based constraints (e.g. Holloway *et al.* [27]), constraint points (e.g. RBF-based method) and constraint normals (e.g. HRBF-based method) are the most common constraints. It is a good strategy to define user-specified contours by converting constraint lines into interpolation constraints (e.g. Ijiri *et al.* [24]). Recently, Yin *et al.* [28] presented an interactive technique that allows the user to edit skeletal curves to prescribe the surface topology. However, new flexible constraint rules need to be developed to control the shape trends.

II. MATHEMATICAL FRAMEWORK

A. PRELIMINARIES

The method relies on the theory of Hermite-Birkhoff interpolation using radial basis functions [3], [9], [29], [30], which is used to deal with the problem of recovering an unknown function f from the linear functional data. The linear functionals involve linear combinations of point evaluations, differentiations, and difference operators that are evaluated on some of the sampling points.

Specifically, the Hermite-Birkhoff interpolation deals with the following situation: Given N distinct points $\{\boldsymbol{x}_1, \boldsymbol{x}_2, \ldots, \boldsymbol{x}_N\}$ and a set of relevant independent linear functionals $L = \{L_1, L_2, \ldots, L_N\}$, we try to construct an interpolant $s(\boldsymbol{x})$ to satisfy the generalized constraints $Ls = Lf$.

If $s(\boldsymbol{x})$ is constructed from a radial basis function interpolant, the generalized interpolant in a real Hilbert space $\mathcal{H}$ of functions has the form [3]

$$s(\boldsymbol{x}) = \sum_{j=1}^{N} \omega_j \lambda_j^{\boldsymbol{x}'} \Phi\left(\boldsymbol{x}, \boldsymbol{x}'\right) + p(\boldsymbol{x}), \quad s \in \mathcal{H} \tag{1}$$

where ω_j are coefficients to be determined, $\lambda_j^{\boldsymbol{x}'}$ are continuous linear functionals acting on a usual radial basis function $\Phi\left(\boldsymbol{x}, \boldsymbol{x}'\right)$ viewed as a function of $\boldsymbol{x}' = (x', y', z')$. When conditionally positive definite functions are used, it is often required to construct low-order polynomials $p(\boldsymbol{x})$ to ensure that the function converges. And the interpolant requires satisfying the orthogonality or side conditions [3]

$$\sum_{j=1}^{N} \omega_j \lambda_j^{\boldsymbol{x}} p_s(\boldsymbol{x}) = 0, \quad 1 \le s \le Q \tag{2}$$

where Q is the number of monomials $p_s(\boldsymbol{x})$. The $(m-1)$ degree trivariate polynomial can be defined as

$$p(\boldsymbol{x}) = \sum_{s=1}^{Q} g_s p_s(\boldsymbol{x}) \tag{3}$$

where g_s are weight coefficients to be determined. In the interpolant, the selection of the degree m depends on the positive definite type of RBF. The condition of positive definiteness is used to ensure the norm-minimal generalized interpolant.

B. EXTENDED HRBF

Let $\delta_{\boldsymbol{x}}$ denotes the point-evaluation functional defined by $\delta_{\boldsymbol{x}}(f) = f(\boldsymbol{x})$. The differential operator [1] $\nabla'_{\boldsymbol{n}}$ can be computed by the derivation of $\Phi\left(\boldsymbol{x}, \boldsymbol{x}'\right)$ with respect to the second variable $\boldsymbol{x}'$. The difference operator [4] Δ'_t can be computed as the difference value of $\Phi\left(x, x'+t\right) - \Phi\left(x, x'-t\right)$ with respect to the second variable x'.

Then we can define the linear functionals $\lambda_j^{\boldsymbol{x}'}$ which operate on the radial basis function $\Phi\left(\boldsymbol{x}, \boldsymbol{x}'\right)$ as

$$\lambda_j^{\boldsymbol{x}'} = \begin{cases} \delta_{\boldsymbol{x}_j'}^{\boldsymbol{x}'}, & j = 1, 2, \ldots, \mu \\ \delta_{\boldsymbol{x}_j'}^{\boldsymbol{x}'} \circ \nabla'_{\boldsymbol{n}}, & j = \mu+1, \mu+2, \ldots, \mu+\sigma \\ \delta_{\boldsymbol{x}_j'}^{\boldsymbol{x}'} \Delta'_{\boldsymbol{t}}, & j = \mu+\sigma+1,\ \mu+\sigma+2, \ldots, \mu+\sigma+\tau \end{cases} \tag{4}$$

where the functionals $\delta_{\boldsymbol{x}_j}^{\boldsymbol{x}'}$ denote point evaluation functionals at $\boldsymbol{x}_j$, $\nabla'_{\boldsymbol{n}}$ are differential operator of gradient and $\Delta'_{\boldsymbol{t}}$ are difference operator along the tangent direction with respect to the second variable $\boldsymbol{x}'$ of $\Phi\left(\boldsymbol{x}, \boldsymbol{x}'\right)$. Similarly, $\delta_{\boldsymbol{x}_j}^{\boldsymbol{x}}$, $\nabla_{\boldsymbol{n}}$ and $\Delta_{\boldsymbol{t}}$ are operators with respect to the first variable $\boldsymbol{x}$.

Based on the definition of the generalized interpolant in Equation (1) and the linear functionals in Equation (4), the expansion of the EHRBF interpolant has the form

$$\begin{aligned} s(\boldsymbol{x}) &= \sum_{j=1}^{N} \omega_j \lambda_j^{\boldsymbol{x}'} \Phi\left(\boldsymbol{x}, \boldsymbol{x}'\right) + p(\boldsymbol{x}) \\ &= \sum_{j=1}^{\mu} a_j \Phi(\boldsymbol{x}, \boldsymbol{x}_j) \\ &\quad + \sum_{k=1}^{\sigma} \langle \boldsymbol{b}_k, \nabla'_{\boldsymbol{n}} \Phi(\boldsymbol{x}, \boldsymbol{x}_{\mu+k}) \rangle \\ &\quad + \sum_{l=1}^{\tau} c_l \Delta'_{\boldsymbol{t}} \Phi\left(\boldsymbol{x}, \boldsymbol{x}_{\mu+\sigma+l}\right) + p(\boldsymbol{x}) \end{aligned} \tag{5}$$

where a_j, c_l are scalar coefficients to be determined and are vector coefficients to be $\boldsymbol{b}_k = (b_{x,k}, b_{y,k}, b_{z,k})$ determined. Similar to the RBF interpolation, the unknown weight coefficients of a_j, $\boldsymbol{b}_k$ and c_l can be determined by solving a linear system. $\langle ., . \rangle$ denotes the inner product of two vectors.

In the problem of the extended HRBF interpolation, we consider the method of surface reconstruction that includes μ domain constraints, σ gradient constraints and τ tangent constraints in N sampling points with point evaluations, differential values or difference values. Among of them, the gradient constraints are vector constraints with three coordinate components.

1) DOMAIN CONSTRAINT

The given μ scattered data points $\{\boldsymbol{x}_i, f(\boldsymbol{x}_i)\}_{i=1}^{i=\mu}$ satisfy

$$f(\boldsymbol{x}_i) = f_i, \quad i = 1, 2, \ldots, \mu \tag{6}$$

where f_i are function values of the domain. Apply the linear functionals $\{\lambda_i^{\boldsymbol{x}}\}_{i=1}^{i=\mu}$ to the interpolant, we can obtain

$$\begin{aligned}\lambda_i^{\boldsymbol{x}} s(\boldsymbol{x}) &= \delta_{\boldsymbol{x}_i}^{\boldsymbol{x}} \circ s(\boldsymbol{x}) \\ &= \sum_{j=1}^{\mu} a_j \overbrace{\Phi(\boldsymbol{x}_i, \boldsymbol{x}_j)}^{\boldsymbol{A}} \\ &\quad + \sum_{k=1}^{\sigma} \overbrace{\left\langle \boldsymbol{b}_k, \nabla_{\boldsymbol{n}}' \Phi(\boldsymbol{x}, \boldsymbol{x}_{\mu+k}) \right\rangle}^{\boldsymbol{B}} \\ &\quad + \sum_{l=1}^{\tau} c_l \overbrace{\Delta_{\boldsymbol{t}}' \Phi(\boldsymbol{x}, \boldsymbol{x}_{\mu+\sigma+l})}^{\boldsymbol{c}} + \overbrace{p(\boldsymbol{x}_i)}^{\boldsymbol{P}}\end{aligned}$$

where the x, y, z components of $\boldsymbol{B} = \left[\boldsymbol{B}_x \ \boldsymbol{B}_y \ \boldsymbol{B}_z\right]$ correspond to the x, y, z components of $\boldsymbol{b}_k$.

The domain constraints according to the different function values can be divided into surface constraints ($f(\boldsymbol{x}_i) = 0$) and off-surface ($f(\boldsymbol{x}_i) \neq 0$) constraints. The off-surface constraints are often obtained by offsetting the contact point along its normal direction. Domain constraints are the basis for defining the domain boundary (zero level set).

2) GRADIENT CONSTRAINT

The given σ scattered data points $\{\boldsymbol{x}_i, \nabla_{\boldsymbol{n}} f(\boldsymbol{x}_i)\}_{i=\mu+1}^{i=\mu+\sigma}$ satisfy

$$\nabla_{\boldsymbol{n}} f(\boldsymbol{x}_i) = \boldsymbol{n}_i, \quad i = \mu+1, \mu+2, \ldots, \mu+\sigma \tag{7}$$

where $\boldsymbol{n}_i = (n_{x,i}, n_{y,i}, n_{z,i})$ are the unit normal vectors of the domain. Apply the linear functionals $\{\lambda_i^{\boldsymbol{x}}\}_{i=\mu+1}^{i=\mu+\sigma}$ to the interpolant, we can obtain

$$\begin{aligned}\lambda_i^{\boldsymbol{x}} s(\boldsymbol{x}) &= \delta_{\boldsymbol{x}_i}^{\boldsymbol{x}} \circ \nabla_{\boldsymbol{n}} s(\boldsymbol{x}) \\ &= \sum_{j=1}^{\mu} a_j \overbrace{\nabla_{\boldsymbol{n}} \Phi(\boldsymbol{x}_i, \boldsymbol{x}_j)}^{\boldsymbol{B}^T} \\ &\quad + \sum_{k=1}^{\sigma} \overbrace{\nabla_{\boldsymbol{n}} \left\langle \boldsymbol{b}_k, \nabla_{\boldsymbol{n}}' \Phi(\boldsymbol{x}, \boldsymbol{x}_{\mu+k}) \right\rangle}^{\boldsymbol{D}} \\ &\quad + \sum_{l=1}^{\tau} c_l \overbrace{\nabla_{\boldsymbol{n}} \Delta_{\boldsymbol{t}}' \Phi(\boldsymbol{x}_i, \boldsymbol{x}_{\mu+\sigma+l})}^{\boldsymbol{E}} + \overbrace{\nabla_{\boldsymbol{n}} p(\boldsymbol{x}_i)}^{\boldsymbol{F}}\end{aligned}$$

where

$$\boldsymbol{D} = \begin{bmatrix} \boldsymbol{D}_{xx} & \boldsymbol{D}_{xy} & \boldsymbol{D}_{xz} \\ \boldsymbol{D}_{yx} & \boldsymbol{D}_{yy} & \boldsymbol{D}_{yz} \\ \boldsymbol{D}_{zx} & \boldsymbol{D}_{zy} & \boldsymbol{D}_{zz} \end{bmatrix}, \quad \boldsymbol{F} = \begin{bmatrix} \boldsymbol{F}_x \\ \boldsymbol{F}_y \\ \boldsymbol{F}_z \end{bmatrix}$$

In the equation, $\nabla_{\boldsymbol{n}} \nabla_{\boldsymbol{n}}'$ and $\nabla_{\boldsymbol{n}} \Delta_{\boldsymbol{t}}'$ are the composition operators. $\boldsymbol{D}$ is the Hessian matrix defined by the second-order partial derivatives of the radial basis functions.

The gradient constraints can be used to define the model direction form the interior to exterior and influence the trend of the adjacent domain. Both gradient and domain constraints can be defined at the same location. They can be taken as soft constraints to control the trend of the domain.

3) TANGENT CONSTRAINT

The given τ scattered data points $\{\boldsymbol{x}_i, \Delta_{\boldsymbol{t}} f(\boldsymbol{x}_i)\}_{i=\mu+\sigma+1}^{i=\mu+\sigma+\tau}$ satisfy

$$\Delta_{\boldsymbol{t}} f(\boldsymbol{x}_i) = 0, \quad i = \mu+\sigma+1, \ \mu+\sigma+2, \ldots, \ \mu+\sigma+\tau \tag{8}$$

where $\boldsymbol{t}_i$ are the real tangent vectors of the domain. The difference values of $\Delta_{\boldsymbol{t}} f(\boldsymbol{x}_i)$ are defined as $f(\boldsymbol{x}_i + \boldsymbol{t}) - f(\boldsymbol{x}_i - \boldsymbol{t})$.

Apply the linear functionals $\{\lambda_i^{\boldsymbol{x}}\}_{i=\mu+\sigma+1}^{i=\mu+\sigma+\tau}$ to the interpolant, we can obtain

$$\begin{aligned}\lambda_i^{\boldsymbol{x}} s(\boldsymbol{x}) &= \delta_{\boldsymbol{x}_i}^{\boldsymbol{x}} \circ \Delta_{\boldsymbol{t}} s(\boldsymbol{x}) \\ &= \sum_{j=1}^{\mu} a_j \overbrace{\Delta_{\boldsymbol{t}} \Phi(\boldsymbol{x}_i, \boldsymbol{x}_j)}^{\boldsymbol{C}^T} \\ &\quad + \sum_{k=1}^{\sigma} \overbrace{\Delta_{\boldsymbol{t}} \left\langle \boldsymbol{b}_k, \nabla_{\boldsymbol{n}}' \Phi(\boldsymbol{x}, \boldsymbol{x}_{\mu+k}) \right\rangle}^{\boldsymbol{E}^T} \\ &\quad + \sum_{l=1}^{\tau} c_l \overbrace{\Delta_{\boldsymbol{t}} \Delta_{\boldsymbol{t}}' \Phi(\boldsymbol{x}_i, \boldsymbol{x}_{\mu+\sigma+l})}^{\boldsymbol{G}} + \overbrace{\Delta_{\boldsymbol{t}} p(\boldsymbol{x}_i)}^{\boldsymbol{H}}\end{aligned}$$

where

$$\boldsymbol{E} = \begin{bmatrix} \boldsymbol{E}_x \\ \boldsymbol{E}_y \\ \boldsymbol{E}_z \end{bmatrix}$$

In the equation, $\Delta_{\boldsymbol{t}} \nabla_{\boldsymbol{n}}'$ and $\Delta_{\boldsymbol{t}} \Delta_{\boldsymbol{t}}'$ are the composition operators.

The tangent constraints can be used to define the direction trend with an unknown polarity of the gradient. Both tangent and domain constraints can be defined at the same location. They can also be taken as soft constraints to control the trend of the domain.

Similarly, for the orthogonality conditions, apply the linear functionals $\{\lambda_i^{\boldsymbol{x}}\}_{i=1}^{i=N}$ to the interpolant, we can obtain

$$\begin{aligned}\lambda_i^{\boldsymbol{x}} p(\boldsymbol{x}) &= (\delta_{\boldsymbol{x}_i}^{\boldsymbol{x}} + \delta_{\boldsymbol{x}_i}^{\boldsymbol{x}} \circ \nabla_{\boldsymbol{n}} + \delta_{\boldsymbol{x}_i}^{\boldsymbol{x}} \circ \Delta_{\boldsymbol{t}}) \circ p(\boldsymbol{x}) \\ &= \sum_{i=1}^{\mu} \overbrace{\sum_{s=1}^{Q} g_s p_s(\boldsymbol{x}_i)}^{\boldsymbol{P}^T} \\ &\quad + \sum_{i=\mu+1}^{\mu+\sigma} \overbrace{\sum_{s=1}^{F^T} g_s \nabla_{\boldsymbol{n}} p_s(\boldsymbol{x}_i)}^{\boldsymbol{F}^T} \\ &\quad + \sum_{i=\mu+\sigma+1}^{\mu+\sigma+\tau} \overbrace{\sum_{s=1}^{Q} g_s \Delta_{\boldsymbol{t}} p_s(\boldsymbol{x}_i)}^{\boldsymbol{H}^T}\end{aligned}$$

C. IMPLEMENTATION

Based on the above analysis, given μ domain constraints, σ gradient constraints and τ tangent constraints for the N

sampling points, it is now possible to construct the following interpolation equation

$$\begin{bmatrix} \boldsymbol{A} & \boldsymbol{B} & \boldsymbol{C} & \boldsymbol{P} \\ \boldsymbol{B}^T & \boldsymbol{D} & \boldsymbol{E} & \boldsymbol{F} \\ \boldsymbol{C}^T & \boldsymbol{E}^T & \boldsymbol{G} & \boldsymbol{H} \\ \boldsymbol{P}^T & \boldsymbol{F}^T & \boldsymbol{H}^T & 0 \end{bmatrix} \begin{bmatrix} \boldsymbol{a} \\ \boldsymbol{b} \\ \boldsymbol{c} \\ \boldsymbol{g} \end{bmatrix} = \begin{bmatrix} \boldsymbol{f} \\ \boldsymbol{n} \\ 0 \\ 0 \end{bmatrix}$$

where $\boldsymbol{a} = \{a_j : 1 \le j \le \mu\}; \boldsymbol{b} = \{b_k : 1 \le k \le \sigma\}; \boldsymbol{c} = \{c_l : 1 \le l \le \tau\}; \boldsymbol{g} = \{g_s : 1 \le s \le Q\}; \boldsymbol{f} = \{f_j : 1 \le j \le \mu\}; \boldsymbol{n} = \{\boldsymbol{n}_k : 1 \le k \le \sigma\}$.

Considering the three components of differential operator, the above linear system can be rewritten as

$$\begin{bmatrix} \boldsymbol{A} & \boldsymbol{B}_x & \boldsymbol{B}_y & \boldsymbol{B}_z & \boldsymbol{C} & \boldsymbol{P} \\ \boldsymbol{B}_x^T & \boldsymbol{D}_{xx} & \boldsymbol{D}_{xy} & \boldsymbol{D}_{xz} & \boldsymbol{E}_x & \boldsymbol{F}_x \\ \boldsymbol{B}_y^T & \boldsymbol{D}_{yx} & \boldsymbol{D}_{yy} & \boldsymbol{D}_{yz} & \boldsymbol{E}_y & \boldsymbol{F}_y \\ \boldsymbol{B}_z^T & \boldsymbol{D}_{zx} & \boldsymbol{D}_{zy} & \boldsymbol{D}_{zz} & \boldsymbol{E}_z & \boldsymbol{F}_z \\ \boldsymbol{C}^T & \boldsymbol{E}_x^T & \boldsymbol{E}_y^T & \boldsymbol{E}_z^T & \boldsymbol{G} & \boldsymbol{H} \\ \boldsymbol{P}^T & \boldsymbol{F}_x^T & \boldsymbol{F}_y^T & \boldsymbol{F}_z^T & \boldsymbol{H}^T & 0 \end{bmatrix} \begin{bmatrix} \boldsymbol{a} \\ \boldsymbol{b}_x \\ \boldsymbol{b}_y \\ \boldsymbol{b}_z \\ \boldsymbol{c} \\ \boldsymbol{g} \end{bmatrix} = \begin{bmatrix} \boldsymbol{f} \\ \boldsymbol{n}_x \\ \boldsymbol{n}_y \\ \boldsymbol{n}_z \\ 0 \\ 0 \end{bmatrix}$$

The determination of interpolant weight coefficients from constraint rules can be accomplished through the solutions of large linear systems. The computational complexity of the extended interpolation algorithm depends on the number of interpolation constraints and the grid resolution for the surface reconstruction. To accelerate the process of dynamical modeling, both of the solution of the linear system and the surface reconstruction must be improved.

The direct method of solving the linear system is the LU decomposition technique, the time complexity of its solution is $O(N^3)$, and the spatial complexity is $O(N^2)$. For $N > 1000$ or more data, it is difficult to address the problem of spatial interpolation of large-scale scattered data. To solve the space and time complexity of large-scale data, two approaches can be used. One is to transform the global interpolation problem into a local interpolation problem, using the compact support radial basis function (CSRBF) method [31]. The interpolation matrix constructed by the local interpolation method is a sparse matrix, which can be solved by the sparse matrix technique. The other is to solve the linear system by fast algorithm. For example, the Krylov subspace iteration method (e.g., GMRES with preconditioners [32]) and fast algorithm (e.g., Fast Multipole Method (FMM) [33], especially kernel independent FMM [34]) are suggested for implementation. In the surface reconstruction of an implicit function, the surface-following method [35], [36] based on the Marching Cubes algorithm is implemented. The method tracks the isosurface using the voxel growing strategy.

III. CONTOURS INTERPOLATION

Given a set of sampling contours $L_1, L_2 \ldots L_k$ on some cutting planes intersecting an unknown surface S, the goal is to reconstruct an implicit function $f(\boldsymbol{x})$ to approximate S whose intersections with the cutting planes coincide with the sampling contours. The implicit surface is defined by the zero level set $\{\boldsymbol{x} | f(\boldsymbol{x}) = 0\}$.

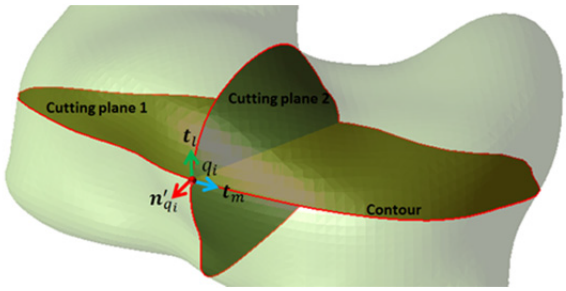

FIGURE 1. Normal estimation based on the linear interpolation of exact normals at intersections. The two contours are located in different cutting planes.

A. NORMAL ESTIMATION

To interpolate the contours, we resample the contours to obtain a set of sampling points $p_1, p_2 \ldots p_M$. The sampling interval can be determined according to the requirements of reconstruction accuracy. The main problem of contour resampling is the estimation of surface normals at the sampling points.

The spatial relationships between the tangent plane of the contours and the model determine the different methods of normal estimation. If the cutting plane of a contour orthogonally intersects with the surface S, the normal vector of the surface S at p_i can be computed as

$$\boldsymbol{n}_{p_i} = Sign_{p_i} \times \frac{(\boldsymbol{t}_{p_i} \times \boldsymbol{c}_{p_i})}{||\boldsymbol{t}_{p_i} \times \boldsymbol{c}_{p_i}||} \tag{9}$$

where $\boldsymbol{t}_{p_i}$ is the tangent vector of the contour at p_i, $\boldsymbol{c}_{p_i}$ is the normal vector of the cutting plane, and $Sign_{p_i}$ is the sign of the normal vector determined by the side of the contour.

The above method is limited to the orthogonal position of the cutting plane. A new approach proposed by Sharma *et al.* [19] can be used to estimate the normal by the orientation of the tangent plane at the intersection, as shown in Figure 1. The normal vector at the intersections between two cross contours can be approximated as

$$\boldsymbol{n}'_{p_i} = \pm \frac{(\boldsymbol{t}_l \times \boldsymbol{t}_m)}{||\boldsymbol{t}_l \times \boldsymbol{t}_m||} \tag{10}$$

where $\boldsymbol{t}_l$ and $\boldsymbol{t}_m$ are tangent vectors of the two cross contours at p_i. The sign of $\boldsymbol{n}'_{p_i}$ can be determined by the sign of $\boldsymbol{n}_{p_i} \cdot \boldsymbol{n}'_{p_i}$. The normals at other points of the corresponding contours can be interpolated linearly by the exactly computed and manually specified normals. Therefore, the real normal vector of the boundary surface at other points can be computed as

$$\boldsymbol{n}_{q_i} = Sign_{q_i} \times \frac{(\boldsymbol{t}_{q_i} \times \boldsymbol{c}'_{q_i})}{||\boldsymbol{t}_{q_i} \times \boldsymbol{c}'_{q_i}||} \tag{11}$$

where $\boldsymbol{c}'_{q_i}$ is the normal vector of the local cutting plane of the contour at q_i. As $\boldsymbol{t}_{q_i}$ is known, we only need to interpolate $\boldsymbol{c}'_{q_i}$ at q_i. Simply, we can use a linear interpolation algorithm to linearly interpolate the approximate normal vector components of the local cutting plane.

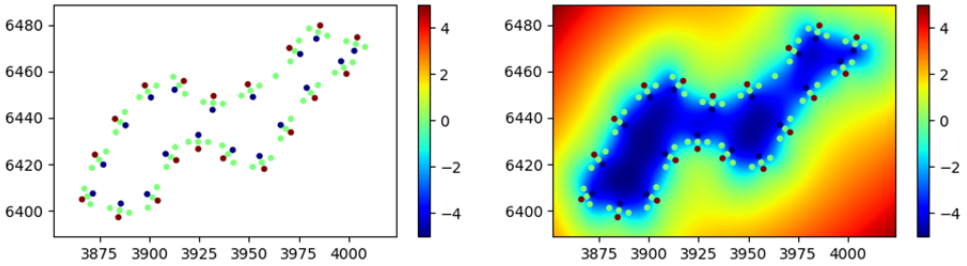

FIGURE 2. Signed distance field analysis of a sampling contour. the geometry domain is sampled by different function values to form a signed distance field representing the distribution of the geometry domain, where red (positive value) represents the exterior of the domain and blue (negative value) represents the interior of the domain.

B. SIGNED DISTANCE FIELD

To construct domain constraints, the function values should be estimated. The distance values can be computed from a set of on-surface and off-surface domain constraints constructed from the signed distance field.

The signed distance value of a point generally uses the Euclidean distance formula to measure the distance to the closest point on the surface. If the point is inside the surface, the distance value is negative, and the distance value is positive if the point is outside the surface. In view of this point, the implicit function of EHRBF can be regarded as a signed distance field function, and the relationship between the implicit function value and the implicit surface ($f(\boldsymbol{x}) = 0$) can be expressed as

$$\begin{cases} \boldsymbol{x}|f(\boldsymbol{x}) = 0, & \boldsymbol{x} \in R^3, \ \textit{on the surface} \\ \boldsymbol{x}|f(\boldsymbol{x}) = +dist\left(\boldsymbol{x}, \boldsymbol{x}'\right) > 0, & \boldsymbol{x} \in R^3, \ \textit{exterior} \\ \boldsymbol{x}|f(\boldsymbol{x}) = -dist\left(\boldsymbol{x}, \boldsymbol{x}'\right) < 0, & \boldsymbol{x} \in R^3, \ \textit{interior} \end{cases}$$

where $\boldsymbol{x} = (x, y, z)$ is a three dimensional sampling point, and $dist\left(\boldsymbol{x}, \boldsymbol{x}'\right)$ is the nearest distance from $\boldsymbol{x}$ to the closest point $\boldsymbol{x}'$ on the surface.

Taking the domain constraints as an example, the reconstruction of the signed distance field is shown in Figure 2. Because the normals of M sampling points have been estimated, we can obtain M on-surface domain constraints and $2M$ off-surface domain constraints by offsetting sampling points along their normal directions. Note that the additional off-surface constraints may cause ambiguity problems when there are thin contours or sharp corners, resulting in inconsistent distance values. To ensure the consistency of the data, an available approach [37] is to validate the distance value at the off-surface point based on the value of its closest point. After solving the EHRBF interpolant, the geometry domain interpolated by constraints is formed, and the level set extracted by the zero function value is the surface of the reconstructed model.

C. INTERACTIVE CONSTRAINTS

In many cases, the spacing between the sparse contours is greater than the spacing between points on a contour. The lack of data support in the sparse domain makes it difficult to reconstruct the continuous trend between contours. Similar to the GRBF interpolant [5], besides constructing the constraints automatically, some interactive constraints can be appended to change the interpolation trend manually, as shown in Figure 3. These user inputs guide the interpolant toward more satisfactory results in different applications.

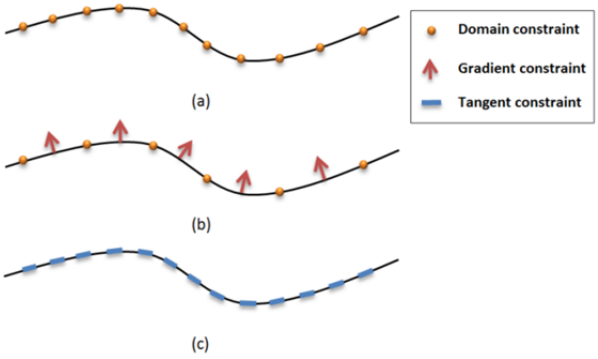

FIGURE 3. Interactive constraints constructed by the interpolation constraints, including (a) constraint line without gradient constraints, (b) constraint line with gradient constraints and (c) trend line.

1) CONSTRAINT LINE

The constraint line refers to the constraint on the boundary surface, which can be used to maintain the local boundary morphological features at the sparse locations with incomplete data.

It can be broken down into two types: orthogonal and non-orthogonal. If the cutting plane of the constraint line orthogonally intersects with the cutting boundary surface of the model, the normal direction of the constraint line can be determined using Equation 10. The constraint line is sampled at a certain point sampling interval to construct domain constraints and sampled at a certain normal sampling interval to construct gradient constraints. If editing a surface with constraint line results in a distorted surface, we can reverse the orientation of the sampling normals to reconstruct the desired surface.

2) TREND LINE

The trend line refers to the constraint that the local connectivity of the model extends in the orientation of the trend line,

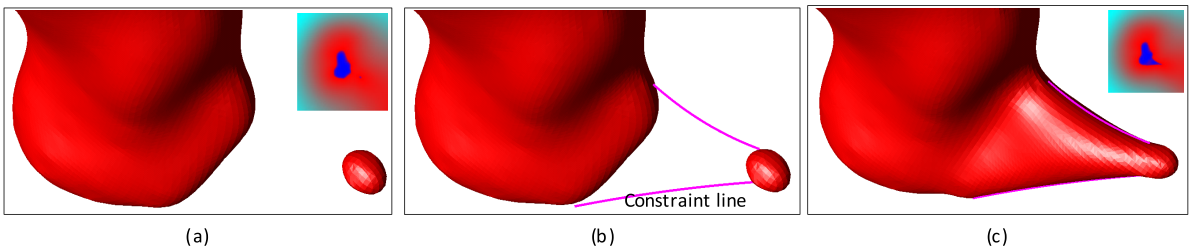

FIGURE 4. An example of specifying constraint lines (b) to maintain the connectivity of the reconstruction (c). Parallel sections tend to create disconnections (a) in sparse data regions. The constraint lines are useful to edit the disconnections.

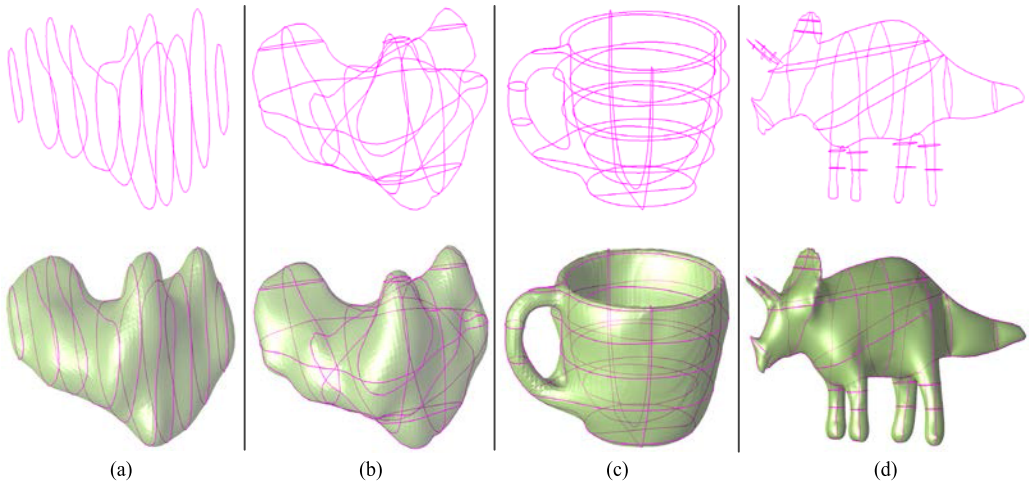

FIGURE 5. Reconstruction from input parallel and non-parallel cross-sections. These data sets are gland1 (parallel) (a), gland2 (non-parallel) (b), mug (c) and triceratops (d).

for which the orientation of the trend line is the tangent vector of the geometry domain.

Given a trend line, it is easy to determine the tangential orientation of the domain at the corresponding location, but it is difficult to determine the gradient orientation. Therefore, we can discretize the trend line into tangent constraints. The trend line can be used as an orientation constraint to guide the model extension trend of nearby domains. Taking the direction of the trend line as the tangential direction, the trend line is sampled at a certain sampling interval to construct tangent constraints. Compared to the normal constraints, tangent constraints do not care about the positive or negative orientations. Therefore, they are very suitable for trend analysis. By specifying trend lines in sparse regions, the reconstruction has a tendency to extend along the trend line.

IV. NUMERICAL RESULTS

We tested the EHRBF interpolant for contours interpolation and the implemented tool on several non-trivial geological and biomedical examples, for which the contours were obtained from the Digital Mine National Lab and Zou *et al.* [22]. These examples contain series of parallel and cross sections in sparse data environments. To validate the performance of this method, we compared the results with existing methods and alternative algorithmic choices.

The extended method can be directly applied to parallel (a) or non-parallel (b) cross sections, as in the gland example shown in Figure 5. The surface reconstruction method, like most other methods, generates model boundary that pass through all contours as it is an exact interpolation method. The mug in Figure 5(c) shows that the exact normal estimation of contours is able to recover the correct topology without any constraints even when the original objects have complex topologies. Finally, we demonstrate the algorithm on a triceratops data set Figure 5(d) made up of 26 non-parallel cross sections.

As shown in Figure 6, compared to the explicit modeling method, the algorithm proposed in this paper could not only reconstruct a smoother surface and high-quality mesh without post-processing, but also has a better robustness and could update the model dynamically.

In the hip example in Figure 7, reconstruction without any geometry constraints leads to topological errors (see arrows in (b) and (c)) using the method of RBF and the method of Liu *et al.* [20] (b). The method of Zou *et al.* [22] can control the topology by incremental sampling; while the quality of the mesh is dependent on the post-processing of refinement and fairing. The EHRBF method does not require post-processing of refinement and fairing, and we can control the degree of model extrapolation by constraint rules.

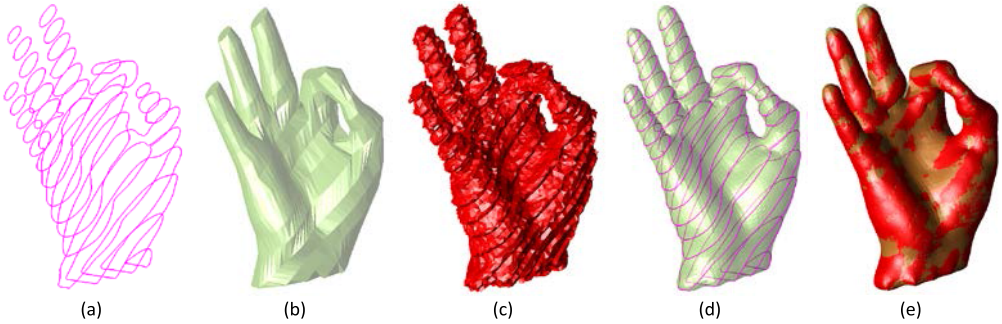

FIGURE 6. Comparison reconstructions from input dense sections (a) using the EHRBF method (d) with the method of explicit modeling (b) and harmonic functions (c). (e) is a comparison of (d) and (c) with post-processing of refinement and fairing.

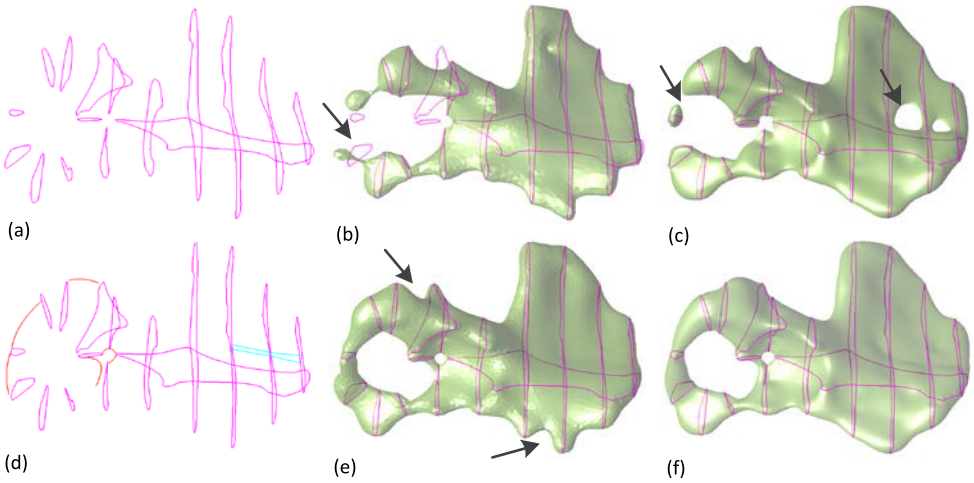

FIGURE 7. Comparison of reconstructions from sparse sections (a) using the method of Lu *et al.* (b), the method of RBF (c), the method of Zou *et al.* [22] (e), and the EHRBF method (f) with constraints of trend lines (in red) and constraint lines (in cyan) (d). Arrows point to unexpected errors, for which the results do not recover the original shape.

TABLE 1. Running time of the solution and reconstruction of the EHRBF method on several examples. The number of constraints, number of vertices, number of polygons, and size of resolution are included in the table.

Model	Constraints	Resolution	Polygons	Time (seconds)			
				Solution	MC	PMC	SF
gland1	1680	1.34	13188	11.89	39.91	10.95	2.71
gland2	1445	4.51	12908	7.95	34.47	9.22	2.27
mug	1965	1.62	23696	18.52	46.29	12.18	5.48
triceratops	2127	0.90	19044	22.38	100.40	25.54	4.98
hip	2080	4.00	23728	21.09	180.19	51.24	6.03

In addition, there are many different constraints on sparse data that can achieve the same trend effect using the improved method. As shown in Figure 7 (d), we used constraint lines to control the topological relationships and trend lines to change the disconnections between contours.

Some more complex examples are shown on geological data in Figure 8. Due to the sparsity in the sections, the reconstructions without tangent constraints using the HRBF interpolant produce excessive extrapolation and undesirable trend in some areas. Based on prior knowledge, the geologists typically construct a large number of additional trend constraints based on supplemental sampling data to guide the local trend of shape. This requires the interpolant to interpolate the trends. For the EHRBF interpolant, we can simply convert these additional constraints as trend lines and dynamically update the model, as shown in Figure 8(c).

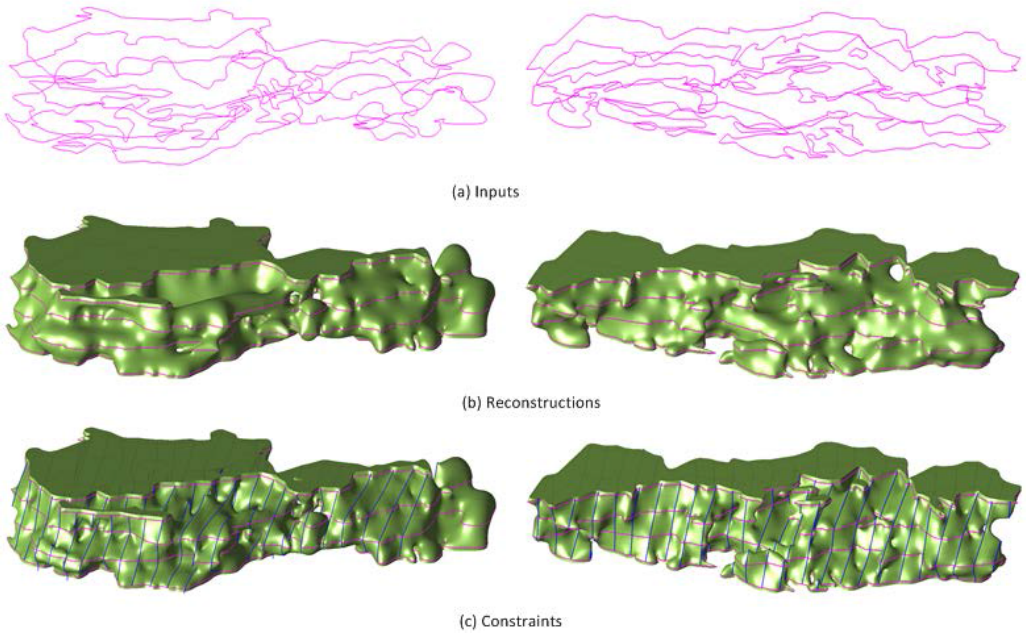

FIGURE 8. The inputs (a) of geological data set and reconstructions without constraints (b) and with constraints (c). The constraints added in (c) are trend lines (in blue).

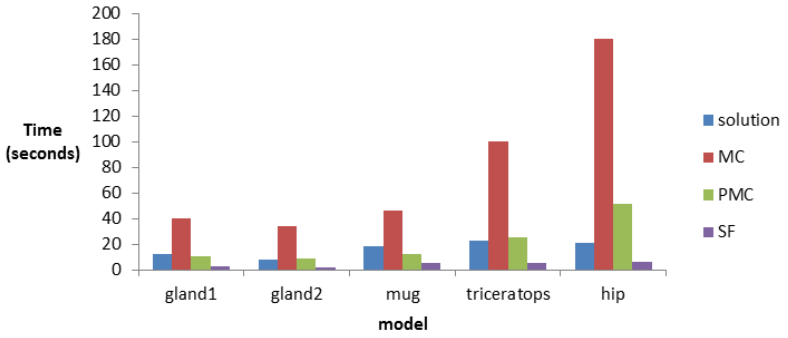

FIGURE 9. Comparison of running time on several examples.

Given μ domain constraints, σ gradient constraints and τ tangent constraints for the $N = \mu + \sigma + \tau$ sampling points, the EHRBF interpolant results in a $(\mu + 3\sigma + \tau) \times (\mu + 3\sigma + \tau)$ linear system. The solution method and surface reconstruction method were implemented in C++. We tested the algorithm on a Windows 64-bit PC with 3.20 GHz Intel(R) Core(TM) i5-3470 and 4GB RAM, as shown in Table 1. The linear system of interpolation constraints was solved using the LU decomposition method directly. The isosurface was extracted using the Marching Cubes (MC) method, the parallel Marching Cubes (PMC) method and the surface following (SF) method.

V. CONCLUSION AND DISCUSSIONS

In this paper, we consider the interpolation or approximation problem that recovers an implicit function from a set of sampling points. Based on the theory of generalized interpolation, the improved interpolant is applied to reconstruct sparse contours that allow the user to manually specify the geometry constraints. It can handle both parallel and non-parallel cross sections flexibly. We extend the RBF interpolant based on the theory of generalized interpolation. The ERBF interpolant has a rich variety of constraint rules which can be converted into general constraints. Combined with the interactive tools of constraint rules, the method gives the user the option to specify various desired model trends. The reconstructed result is a geometrically valid model meeting the requirements of the specified interpolation trend. The method also has extraordinary extrapolation capabilities, even when large gaps occur in the sections.

A. LIMITATIONS

The method has several limitations that await further investigation and improvement. Similar to the HRBF interpolant, the main limitation of the method is its relatively high computational cost. As mentioned earlier, the performance can be

improved by using the compactly-supported RBFs. However, it changes the global interpolation effect of the interpolant, which was investigated by Macedo *et al.* [1]. It is necessary to develop a fast global method for the EHRBF interpolant. In contrast, the solution time of the gradient constraints is nine times that of the domain constraints or the tangent constraints. It is recommended to use less gradient constraints.

The result of surface reconstruction from sparse sections depends to a large extent on the accuracy of the contour normal estimation. The method of normal estimation does not consider the shape trend and the topological relationship between the contours. This problem could be solved if an underlying image volume is available in specific applications. As in (Ijiri *et al.*, 2013 [24]), the direction of the normals can be oriented along the image intensity gradient. However, it only works well around image areas with high-contrast edges. Without priori contour information, although a variety of normal estimation methods have been proposed, it is still difficult to accurately estimate the true normal due to the sparsity of the contours. The method of normal estimation should be optimized in future works to avoid undesirable artifacts.

B. EXTENSIONS

As the implicit function has the advantage of easily determining the internal and external relationships of the model, we can extend the method to the computational modeling of multi-labeled domains by defining the rules of multi-labeled material interfaces. The complex multi-domains can be reconstructed using the Boolean operations such as union, intersection, and subtraction, according to the modeling sequence.

Another direction for future extension is to construct the constraint rules automatically according to the data properties and features. For example, according to the sparseness of the model, the local varying anisotropy constraints that reflect the trend of the continuity of the model can be automatically constructed. In addition, we have already started to explore other constraint rules by converting into general constraints. In particular, the constraint rules for topological controls are useful to fix the undesired topological errors. We will continue to explore ways in which the approach can be extended to offer more extensive and flexible trend controls over the geometry domain.

REFERENCES

[1] I. Macêdo, J. P. Gois, and L. Velho, "Hermite radial basis functions implicits," *Comput. Graph. Forum*, vol. 30, no. 1, pp. 27–42, Mar. 2011.

[2] R. Pan, X. Meng, and T. Whangbo, "Hermite variational implicit surface reconstruction," *Sci. China F, Inf. Sci.*, vol. 52, no. 2, pp. 308–315, Feb. 2009.

[3] H. Wendland, *Scattered Data Approximation*. Cambridge, U.K.: Cambridge Univ. Press, 2004.

[4] D.-Y. Zhong, L.-G. Wang, and L. Bi, "Implicit surface reconstruction based on generalized radial basis functions interpolant with distinct constraints," *Appl. Math. Model.*, vol. 71, pp. 408–420, Jul. 2019.

[5] D.-Y. Zhong, L.-G. Wang, L. Bi, and M.-T. Jia, "Implicit modeling of complex orebody with constraints of geological rules," *Trans. Nonferrous Met. Soc. China*, vol. 29, no. 11, pp. 2392–2399, Nov. 2019.

[6] F. Calakli and G. Taubin, "SSD: Smooth signed distance surface reconstruction," *Comput. Graph. Forum*, vol. 30, no. 7, pp. 1993–2002, Sep. 2011.

[7] G. M. Nielson, "On marching cubes," *IEEE Trans. Vis. Comput. Graphics*, vol. 9, no. 3, pp. 283–297, Jul. 2003.

[8] J. Bloomenthal and B. Wyvill, "Interactive techniques for implicit modeling," *ACM SIGGRAPH Comput. Graph.*, vol. 24, no. 2, pp. 109–116, Mar. 1990.

[9] W. Zongmin, "Hermite-Birkhoff interpolation of scattered data by radial basis functions," *Approx. Theory Appl.*, vol. 8, no. 2, pp. 1–10, Jun. 1992.

[10] H. C. Batagelo and J. P. Gois, "Least-squares Hermite radial basis functions implicits with adaptive sampling," in *Proc. Graph. Interface*, Regina, SK, Canada, May 2013, pp. 109–116.

[11] S. Liu, C. C. L. Wang, G. Brunnett, and J. Wang, "A closed-form formulation of HRBF-based surface reconstruction by approximate solution," *Comput.-Aided Des.*, vol. 78, pp. 147–157, Sep. 2016.

[12] S. Cuomo, A. Galletti, G. Giunta, and L. Marcellino, "Reconstruction of implicit curves and surfaces via RBF interpolation," *Appl. Numer. Math.*, vol. 116, pp. 157–171, Jun. 2017.

[13] A. de Boer, M. S. van der Schoot, and H. Bijl, "Mesh deformation based on radial basis function interpolation," *Comput. Struct.*, vol. 85, nos. 11–14, pp. 784–795, Jun. 2007.

[14] G. Casciola, D. Lazzaro, L. B. Montefusco, and S. Morigi, "Shape preserving surface reconstruction using locally anisotropic radial basis function interpolants," *Comput. Math. Appl.*, vol. 51, no. 8, pp. 1185–1198, Apr. 2006.

[15] M. J. Hillier, E. M. Schetselaar, E. A. de Kemp, and G. Perron, "Three-dimensional modelling of geological surfaces using generalized interpolation with radial basis functions," *Math. Geosci.*, vol. 46, no. 8, pp. 931–953, Nov. 2014.

[16] S. Ettl, J. Kaminski, and G. Häusler, "Generalized Hermite interpolation with radial basis functions considering only gradient data," in *Curve and Surface Design: Avignon 2006*. 2017, pp. 141–149.

[17] J. P. Gois, D. F. Trevisan, H. C. Batagelo, and I. Macêdo, "Generalized hermitian radial basis functions implicits from polygonal mesh constraints," *Vis. Comput.*, vol. 29, nos. 6–8, pp. 651–661, Jun. 2013.

[18] K. Liu, M. Xu, and Z. Yu, "Adaptive mesh representation and restoration of biomedical images," 2014, *arXiv:1406.7062*. [Online]. Available: http://arxiv.org/abs/1406.7062

[19] O. Sharma and N. Agarwal, "Signed distance based 3D surface reconstruction from unorganized planar cross-sections," *Comput. Graph.*, vol. 62, pp. 67–76, Feb. 2017.

[20] L. Liu, C. Bajaj, J. O. Deasy, D. A. Low, and T. Ju, "Surface reconstruction from non-parallel curve networks," *Comput. Graph. Forum*, vol. 27, no. 2, pp. 155–163, Apr. 2008.

[21] C. Shen, J. F. O'Brien, and J. R. Shewchuk, "Interpolating and approximating implicit surfaces from polygon soup," in *Proc. ACM SIGGRAPH*, 2005, p. 204.

[22] M. Zou, M. Holloway, N. Carr, and T. Ju, "Topology-constrained surface reconstruction from cross-sections," *ACM Trans. Graph.*, vol. 34, no. 4, p. 128, Jul. 2015.

[23] A. Bermano, A. Vaxman, and C. Gotsman, "Online reconstruction of 3D objects from arbitrary cross-sections," *ACM Trans. Graph.*, vol. 30, no. 5, pp. 1–11, Oct. 2011.

[24] T. Ijiri, S. Yoshizawa, Y. Sato, M. Ito, and H. Yokota, "Bilateral Hermite radial basis functions for contour-based volume segmentation," *Comput. Graph. Forum*, vol. 32, no. 2, pp. 123–132, May 2013.

[25] Z. Huang, M. Zou, N. Carr, and T. Ju, "Topology-controlled reconstruction of multi-labelled domains from cross-sections," *ACM Trans. Graph.*, vol. 36, no. 4, pp. 1–12, Jul. 2017.

[26] S.-U. Kim and C.-O. Lee, "Accurate surface reconstruction in 3D using two-dimensional parallel cross sections," *J. Math. Imag. Vis.*, vol. 53, no. 2, pp. 182–195, Oct. 2015.

[27] M. Holloway, C. Grimm, and T. Ju, "Template-based surface reconstruction from cross-sections," *Comput. Graph.*, vol. 58, pp. 84–91, Aug. 2016.

[28] K. Yin, H. Huang, H. Zhang, M. Gong, D. Cohen-Or, and B. Chen, "Morfit: Interactive surface reconstruction from incomplete point clouds with curve-driven topology and geometry control," *ACM Trans. Graph.*, vol. 33, no. 6, pp. 202:1–202:12, Nov. 2014.

[29] G. Fasshauer, "Meshfree methods," in *Handbook of Theoretical and Computational Nanotechnology*. New York, NY, USA: American Scientific Publishers, 2005.

[30] G. E. Fasshauer, *Meshfree Approximation Methods With MATLAB*. London, U.K.: World Scientific, 2007.

[31] V. Skala, "RBF interpolation with CSRBF of large data sets," *Procedia Comput. Sci.*, vol. 108, pp. 2433–2437, Jan. 2017.
[32] N. A. Gumerov and R. Duraiswami, "Fast radial basis function interpolation via preconditioned Krylov iteration," *SIAM J. Sci. Comput.*, vol. 29, no. 5, pp. 1876–1899, Jan. 2007.
[33] R. Yokota, L. A. Barba, and M. G. Knepley, "PetRBF—A parallel O(N) algorithm for radial basis function interpolation with Gaussians," *Comput. Methods Appl. Mech. Eng.*, vol. 199, nos. 25–28, pp. 1793–1804, May 2010.
[34] D. Malhotra and G. Biros, "PVFMM: A parallel kernel independent FMM for particle and volume potentials," *Commun. Comput. Phys.*, vol. 18, no. 3, pp. 808–830, Sep. 2015.
[35] T.-Y. Lee and C.-H. Lin, "Growing-cube isosurface extraction algorithm for medical volume data," *Comput. Med. Imag. Graph.*, vol. 25, no. 5, pp. 405–415, Sep. 2001.
[36] X. Wang, Y. Niu, L.-W. Tan, and S.-X. Zhang, "Improved marching cubes using novel adjacent lookup table and random sampling for medical object-specific 3D visualization," *J. Softw.*, vol. 9, no. 10, Oct. 2014.
[37] J. C. Carr, R. K. Beatson, J. B. Cherrie, T. J. Mitchell, W. R. Fright, B. C. McCallum, and T. R. Evans, "Reconstruction and representation of 3D objects with radial basis functions," in *Proc. 28th Annu. Conf. Comput. Graph. Interact. Techn. (SIGGRAPH)*, Los Angeles, CA, USA, 2001, pp. 67–76.

DEYUN ZHONG received the bachelor's degree from Central South University, in 2013, and the M.S. degree from Fuzhou University, in 2016. He is currently pursuing the Ph.D. degree with Central South University. His current research interests include geological statistics, geology modeling, surface reconstruction, geometry processing, and their applications.

LIGUAN WANG received the M.S. degree from Central South University, China, in 1988, and the Ph.D. degree from Akita University, Japan, in 2002. He is currently a Professor with Central South University. His current research interests mainly focused on digital mine, geology modeling, rock mechanics, and their applications.

LIN BI received the M.S. degree from the China University of Geosciences, in 2006, and the Ph.D. degree from Central South University, in 2010. He is currently an Associate Professor with Central South University. His research interests include digital mine, geology modeling, simultaneous localization and mapping, and their applications.